CrossMark

Synthesis and electromagnetic absorption properties of Fe_3O_4@C nanofibers/bismaleimide nanocomposites

Qi Yu[1] · Hanlin Chen[1] · Ping Chen[2] · Qi Wang[1] · Chun Lu[1] · Caixia Jia[1]

Abstract Carbon nanofibers containing Fe_3O_4 nanoparticles (Fe_3O_4@C nanofibers) were synthesized by electrospinning technique followed by heat treatment, and then the as-prepared nanofibers were loaded in bismaleimide (BMI) resin to prepare nanocomposites. The phase structure and morphology of nanofibers were characterized by X-ray diffraction and scanning electron microscope, respectively. The complex permittivity and permeability of nanocomposites were measured by vector network analyzer using a coaxial line method in the frequency range of 1–18 GHz, and the microwave absorption performance was accordingly evaluated. The results indicated that the Fe_3O_4@C nanofibers/BMI composites showed excellent low-frequency electromagnetic wave absorption properties with a minimum RL value of −22 dB at 2.1 GHz corresponding to a thickness of 6 mm and exceeding −10 dB with thickness of 3–6 mm in the whole S band (2–4 GHz). The strong absorption in low frequency is attributed to good matching characteristics of dielectric loss and magnetic loss, which can be efficiently tailored by combination of magnetic Fe_3O_4 and dielectric carbon layer through electrospining technology. The novel Fe_3O_4@C nanofibers loaded in BMI resin can provide an effective solution for pressing problem in present that how to produce lightweight microwave absorbing nanocomposites with excellent low-frequency electromagnetic absorption properties.

1 Introduction

Microwave absorption materials based upon polymer nanocomposites are widely used as stealth coating or resin matrix for structural absorbing composites, which play a particular important role in civil and military applications [1–6]. The incorporation of magnetic nanoparticles into polymer matrix is capable of endowing the nanocomposites with enhanced physical properties and microwave absorption properties. Fe_3O_4 nanoparticles are a kind of magnetic materials with inexpensive, non-toxic and paramagnetic characteristic, which have been widely used as microwave absorption materials [7–10]. Unfortunately, their high-density can hardly meet the requirement of lightweight on absorption materials, thus restricts their universal applications.

Electrospinning is a novel and highly efficient technique providing a versatile approach to produce carbon nanofibers, which have gained more attention due to their convenience in preparation and low costs in production [11–14]. Confining magnetic nanoparticles in carbon nanofibers by electrospinning technology not only can enhance their impedance matching characteristic, but also produce magnetic nanoparticles with low-dimension, microporosity and large specific surface area, thereby promoting the absorbing ability per unit mass [15–19]. Simultaneously, if the Fe_3O_4 nanoparticles are made into carbon nanofibers, it will have lower specific gravity owing to a larger specific surface area. Therefore, as a new kind of microwave absorber, magnetic metal nanoparticles

✉ Ping Chen
  chenping_898@126.com

1 School of Aerospace Engineering and Liaoning Key Laboratory of Advanced Polymer Matrix Composites, Shenyang Aerospace University, Shenyang 110136, China

2 School of Chemical Engineering and State Key Laboratory of Fine Chemicals, Dalian University of Technology, Dalian 116024, China

enveloped in carbon nanofibers are capable of meeting the comprehensive requirements of light weight, strong absorption, thin thickness and broadband on absorption materials. Furthermore, it is necessary to pay special attention to fabricate polymer resin loaded with novel Fe_3O_4@C nanofiber absorbers aiming at seeking efficient stealth coating or resin matrix for structural absorbing composites applied in aerospace engineering.

In this work, Fe_3O_4@C nanofibers were synthesized by electrospinning technique followed by heat treatment, and then the as-prepared nanofibers were loaded in BMI resin to prepare nanocomposites. The phase structure and morphology of nanofibers were characterized by X-ray diffraction (XRD) and scanning electron microscope (SEM), respectively. The complex permittivity and permeability of nanofibers/BMI nanocomposites were measured by vector network analyzer using a coaxial line method in the frequency range of 1–18 GHz, and the microwave absorption performance was accordingly evaluated.

2 Experimental

Firstly, Fe_3O_4@C nanofibers were synthesized via electrospinning followed by stabilization and carbonization processes. 1.2 g of polyvinylpyrrolidone (PVP, Mw = 1,300,000, Aladdin Industrial Co.) was dissolved in a mixture of 10 g of ethyl alcohol and 5 g of deionized water under mechanical stirring at room temperature for 1 h to form homogeneous solution. 0.18 g of acetyl acetonate iron (AAI, purchased from Chengdu Huaxia Chemical Co.) was then added into the solution and stirred for another 1 h. Subsequently, the precursor solution (10 ml) was loaded into a plastic syringe with a stainless steel needle (0.7 mm in inner diameter). The needle used as the positive electrode was connected to a high-voltage supply. During the electrospinning, the applied voltage was kept at 18 kV, when the distance between the spinneret and a metal collector was optimized and around 10 cm. The composite nanofibers in the form of non-woven mats were initially dried for 1 h at 100 °C, and then calcined at different temperatures (600, 700 and 800 °C) for 2 h in the argon atmosphere with a heating rate of 3 °C/min. Afterwards, 50 wt% as-prepared nanofibers and 50 wt% BMI resin (QY8911-II, AVIC Beijing Aeronautical Manufacturing Technology Research Institute) were mixed homogeneously and then were melted and degassed under reduced pressure to remove any volatiles or entrapped air. Thereafter, the hybrids were injected into a preheated mold and thermally cured in an air convection oven. The heating schedule was as follows: 145 °C for 1 h, 210 °C for 3 h, and 255 °C for 3 h.

Phase composition of the nanofibers was analyzed by X-ray diffraction (XRD) with conditions of Cu-K$_\alpha$ signal, continuous scanning mode with a speed of 8°/min and a

step of 0.02°, 2θ from 20° to 90°. The morphologies and microstructures of the nanofibers were observed by a scanning electron microscopy (SEM, SU3500). Nanofibers diameter were determined by analysis of SEM images manually. The nanofibers/BMI composites were cut into the toroidal test specimen (7 mm in outer diameter, 3 mm in inner diameter and 3 mm in thickness) to measure the complex permittivity and permeability by a coaxial line method in the frequency range of 1–18 GHz using a Vector Network Analyzer (8720ET). The reflection losses (R$_L$) of the nanocomposites were calculated by Matlab based on the relatively complex permeability and permittivity at a given frequency and matching thickness according to the following equations:

$$Z_{in} = Z_0 \sqrt{\frac{\mu_r}{\varepsilon_r}} \tanh \left[j\left(\frac{2\pi f d}{c}\right) \sqrt{\mu_r \varepsilon_r} \right] \qquad (1)$$

$$RL(\text{dB}) = 20 \log_{10} \left| \frac{Z_{in} - Z_0}{Z_{in} + Z_0} \right| \qquad (2)$$

where f is the frequency of the electromagnetic wave, d is the coating thickness, c is the velocity of light, Z_0 is the impedance of free space, and Z_{in} is the input impedance of the absorber.

3 Results and discussion

3.1 Phase structure and morphology of nanofibers

Figure 1 shows the XRD patterns of Fe_3O_4@C nanofibers calcined under different temperatures from 600 to 800 °C. It can be observed that the diffraction peaks and relatively
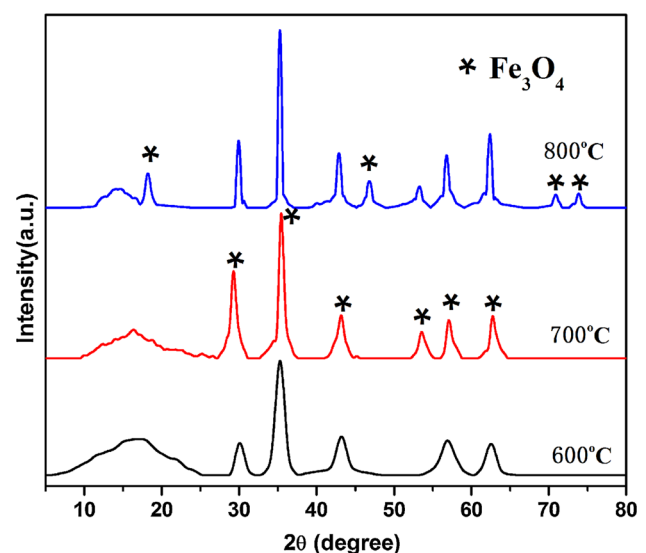

Fig. 1 XRD pattern of electrospun Fe_3O_4@C nanofibers calcined at different temperature: **a** 600 °C, **b** 700 °C, **c** 800 °C

intensities appearing in all XRD patterns with 2θ at 18.1°, 30.4°, 35.7°, 43.3°, 57.2°, 62.8° standing for (110), (220), (311), (400), (511) and (440), respectively, are in good accordance with the standard peaks of Fe_3O_4 (JCPDS No. 65-3107). When the calcination temperature increases from 600 to 700 °C, there is a new diffraction peak detected with 2θ at 53.4° in XRD which is assigned to the crystal plane of Fe_3O_4. When the calcination temperature is 800 °C, some new diffraction peaks appearing with 2θ at 46.3°, 70.8° and 73.9° can also be assigned to the new formation of Fe_3O_4 phase. Meanwhile, the Fe_3O_4 diffraction peaks become narrower and higher with increasing calcination temperature. These observations indicate that the crystallinity increases and the grains become bigger at a higher calcination temperature of 800 °C. Additionally, the wide diffraction peak at $2\theta = 17.5°$ is assigned to amorphous carbon, indicating that the obtained hybrid nanofibers consist of carbon and Fe_3O_4 phase.

Figure 2 shows SEM images of electrospun precursor nanofibers and Fe_3O_4@C nanofibers calcined at 800 °C. It can be observed from Fig. 2a that the electrospun AAI/
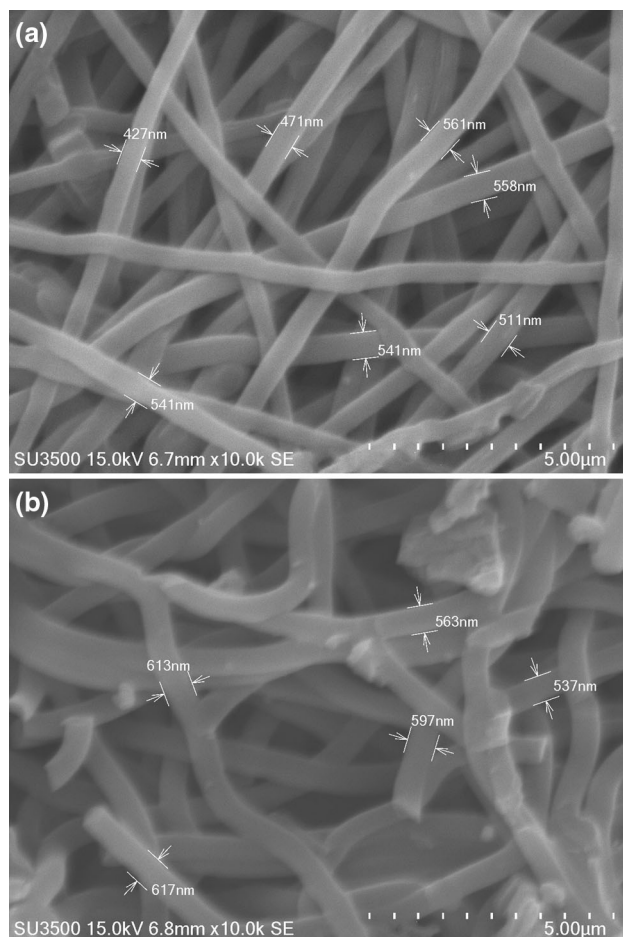

Fig. 2 SEM images of **a** electrospun precursor nanofibers and **b** Fe_3O_4@C nanofibers calcined at 800 °C

PVP precursor nanofibers have shown interpenetrating networks structure consisted of superfine fibers in microscopic view. The precursor nanofibers have a smooth surface and are uniform in size with the diameter ranging from 420 to 560 nm. As seen from Fig. 2b, the Fe_3O_4@C nanofibers still maintain well-defined nanofibrous morphology with the diameter ranging from 530 to 620 nm after carbonization at 800 °C. However, it is obvious that there are more fracture occurring and more protrusions formed on the fiber surface after carbonization. It is because that the heat treatment process would induce thermal stress concentration at local region in nanofibers where the Fe_3O_4 nanoparticles tends to form aggregation, therefore, the nanofibers bear more stress and easily cause fracture.

3.2 Permittivity and permeability of nanocomposites

Figure 3a shows the frequency dependence of the real part (ε') and imaginary part (ε'') of complex permittivity for BMI composites with 50 wt% Fe_3O_4@C nanofibers loading. It can be observed that the ε' decreases from 31.3 to 14.1, while the ε'' exhibits an opposite variation trend increasing from 4.8 to 16.1 with increasing frequency from 1 to 18 GHz. Generally, the real parts (ε') and imaginary parts (ε'') of complex permittivity are related to polarization and loss capability in electric field, respectively. The higher complex permittivity including ε' and ε'' are attributed to the Fe_3O_4@C nanofibers loaded in BMI resin matrix, which introduce dissipation due to polarization processes involving space charge polarization, dipole polarization and interfacial polarization at microwave band. For the metal-based nanocomposites, the nanofibers with unsaturated bonds on surface could be considered as dipoles, which would bring about dipole polarization and space charge polarization in the electric field. Meanwhile, both ends of interface including Fe_3O_4 nanoparticles and carbon layer as well as carbon layer and BMI resin matrix exist different electric potential, which would induce charge accumulation at the interface and thus the interfacial polarization is greatly enhanced. As the frequency increases, the polarization responses begin to lag behind the change of electromagnetic wave, thereby inducing the decrease in the ε' and the increase in the ε''.

Figure 3b shows the frequency dependence of the real part (μ') and imaginary part (μ'') of complex permeability for Fe_3O_4@C nanofibers/BMI composites. The real parts (μ') and imaginary parts (μ'') of complex permeability represent the storage capability and loss of magnetic energy, respectively. From Fig. 3b, the μ' is found to decline from 1.2 to 0.75 with increasing frequency from 1 to 18 GHz, with several resonance peaks observed at
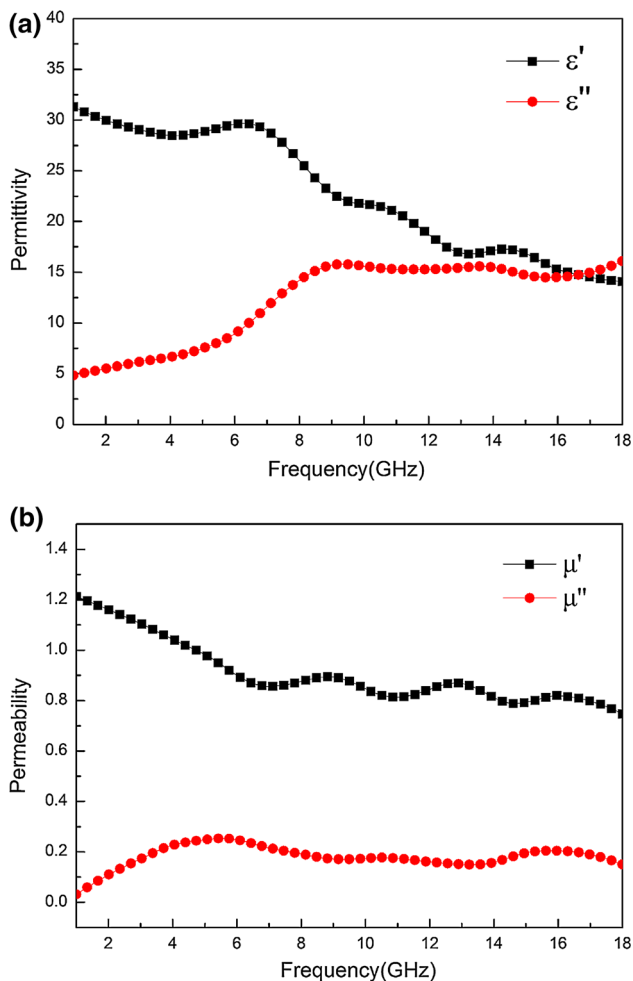
Fig. 3 Frequency dependence of real part and imaginary part of relative complex, **a** permittivity and **b** permeability for Fe_3O_4@C nanofibers/BMI composite

Fig. 4 a Values of $\mu''(\mu')^{-2}f^{-1}$ for the Fe_3O_4@C nanofibers/BMI composite versus frequency. **b** Frequency dependence of dielectric loss and magnetic loss tangent for Fe_3O_4@C nanofibers/BMI composite

8.5–9.2, 12.8–13.5 and 15.8–16.2 GHz. Correspondingly, the μ'' values initially increase from 0.03 to 0.25 at 1–5.8 GHz, and then decrease and keep relatively constant at around 0.2 with increasing frequency from 5 to 18 GHz. The multi-resonance behavior observed in the μ' and μ'' curves are ascribed to the magnetic Fe_3O_4 nanoparticles enveloped in carbon, which could introduce magnetic loss mechanisms including domain-wall resonance, natural resonance, exchange resonance and eddy current loss. However, the domain-wall resonance generally doesn't occur in GHz band. The eddy current loss can be expressed by the equation $\mu''(\mu')^{-2}f^{-1} = 2\pi\mu_0 d^2\sigma$, which is related to the thickness d and the electric conductivity σ as seen from the right side of the equation. Consequently, the values of $\mu''(\mu')^{-2}f^{-1}$ should be a constant in the frequency range from 1 to 18 GHz. From Fig. 4a, it can be observed that the values of $\mu''(\mu')^{-2}f^{-1}$ change large in the measured frequency range, indicating that the eddy current loss can be eliminated. The natural resonance can be expressed by
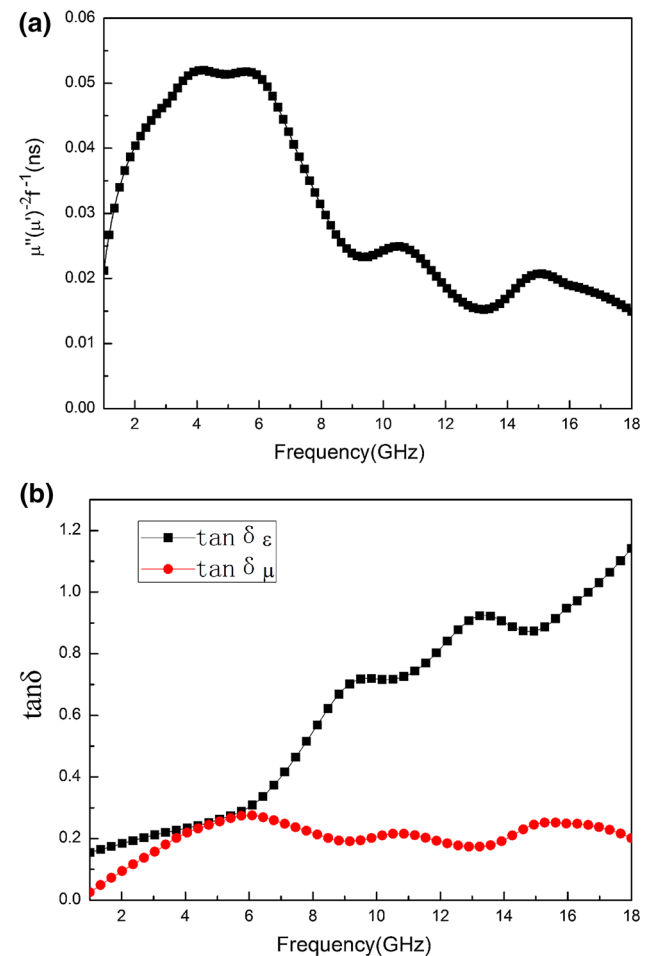
$f = \gamma H_A/2\pi$, where γ is the gyromagnetic ratio and the H_A is the effective magnetic anisotropy field. Thus, the natural resonance depends strongly on the effective magnetic anisotropy field, which can be significantly enhanced by the smaller particle size. Consequently, the nanoscale Fe_3O_4@C fibers own higher effective magnetic anisotropy field, thus makes the natural resonance exert an important influence on the complex permeability at microwave band. Simultaneously, it is possible to appear exchange resonance due to small size effects of nanofibers. The natural resonance and exchange resonance which play a major role in microwave region, will always cause the decrease in the μ' with increasing frequency [20], that has been verified by the μ' curve as shown in Fig. 3b.

Figure 4b shows the dielectric loss tangent (tan $\delta_\varepsilon = \varepsilon''/\varepsilon'$) and the magnetic loss tangent (tan $\delta_\mu = \mu''/\mu'$) of Fe_3O_4@C nanofibers/BMI composites. It can be observed that the tan δ_ε values obviously increase from 0.15 to 1.1 with increasing frequency, while the tan δ_μ curve becomes

relatively flat in the whole frequency range with the values increasing from around 0.03 to 0.2. The dielectric losses induced by multiple polarization processes of $Fe_3O_4@C$ nanofibers loaded in BMI resin matrix mainly include space charge polarization, dipole polarization and interfacial polarization, which are obviously enhanced with increasing frequency due to the gradually lag of polarization responses behind the change of electromagnetic wave. While the magnetic loss induced by natural resonance and exchange resonance mostly depends on the magnetic Fe_3O_4 component of nanofibers, that is relatively low compared with the dielectric loss especially at 8–18 GHz. Thus, the microwave absorption of the nanocomposites results mainly from dielectric loss rather than magnetic loss in higher frequency region. However, it is not always good for microwave absorption materials possessing higher dielectric loss and lower magnetic loss, which will lead to surface impedance mismatch by causing incident microwave reflected on the surface rather than absorbed in the material. It can be observed from Fig. 4 that the values of tan δ_ε at 3–7 GHz are closer to that of tan δ_μ, indicating a better balance between dielectric loss and magnetic loss and thus results in an enhanced microwave absorption performance in low frequency region. Therefore, the good matching characteristics of dielectric loss and magnetic loss can be efficiently tailored by the microstructure of composite nanofibers consisting of magnetic Fe_3O_4 nanoparticles enveloped in dielectric carbon layer, which is benefit to improve the microwave absorption performance of the $Fe_3O_4@C$ nanofibers modifying BMI nanocomposites.

3.3 Microwave absorption properties of nanocomposites

To further reveal the microwave absorption properties of BMI composites with 50 wt% $Fe_3O_4@C$ nanofibers loading, the reflection loss (RL) of the nanocomposites were calculated from relatively permittivity and permeability at given frequency and matching thickness according to transmission line theory. Figure 5 shows the relationship between the RL and the microwave frequency in the 1–18 GHz range for the nanocomposites with different thicknesses. It can be observed that the peak of RL curves obviously shifts to lower frequency with increasing thickness, accompanied with the width of absorption peak getting narrow. Simultaneously, the intensity of absorption peak significantly increases firstly and then decrease with increasing thickness. Generally, the RL values exceeding −10 dB means that more than 90 % of the incident electromagnetic wave is absorbed correspondingly. It can be observed from Fig. 5 that when the thickness of nanocomposite increases from 3.0 to 6.0 mm, the
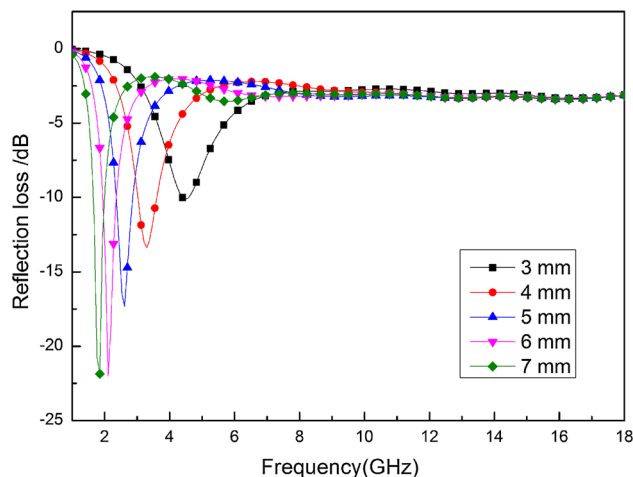

Fig. 5 Reflection loss (RL) curves versus frequency of $Fe_3O_4@C$ nanofibers/BMI composite

minimum RL value obviously increases from −10.1 dB at 4.5 GHz to −22 dB at 2.1 GHz. However, as the thickness further increases to 7.0 mm, the minimum RL value decreases to −21.3 dB at 1.8 GHz. It can be concluded that $Fe_3O_4@C$/BMI composites have excellent microwave absorption properties in low frequency region especially at 2–4 GHz, which can provide an effective solution for pressing problem in present that how to produce microwave absorption material aiming to improve the weak absorption performance in the low frequency waveband range. Furthermore, increasing thickness of nanocomposites which results in the absorption peak moving towards left, is better for improving the absorbing properties in lower frequency. However, further increase in the thickness could induce mismatch of dielectric loss and magnetic loss, thereby leading to a reduced microwave absorption properties. Therefore, excellent microwave absorption properties not only depends on higher dielectric and magnetic loss but also the good electromagnetic matching, which can make microwave enter into the material interior and dissipated rather than reflected on the material surface.

4 Conclusions

$Fe_3O_4@C$ nanofibers were synthesized by electrospinning technique followed by heat treatment, and then the as-prepared nanofibers were loaded in BMI resin to prepare $Fe_3O_4@C$ nanofibers/BMI nanocomposites. SEM images show that the diameter of the $Fe_3O_4@C$ nanofibers ranges from 530 to 620 nm. The $Fe_3O_4@C$ nanofibers/BMI composites show excellent low-frequency electromagnetic wave absorption properties with a minimum RL value of −22 dB at 2.1 GHz corresponding to a thickness of 6 mm and exceeding −10 dB with thickness of 3–6 mm in the

whole S band (2–4 GHz). The strong absorption in low frequency is attributed to good matching characteristics of dielectric loss and magnetic loss, which can be efficiently tailored by combination of magnetic Fe_3O_4 and dielectric carbon layer through electrospinning technology. These results indicate that the novel Fe_3O_4@C nanofibers loaded in BMI resin can provide an effective solution for pressing problem in present that how to produce lightweight microwave absorbing nanocomposites with excellent low-frequency electromagnetic absorption properties.

References

1. M.S. Shi, H. Huang, C.J. Xie, F.H. Xue, P. Chen, X.L. Dong, CJJCC. **10**, 267 (2012)
2. L.M. Yu, B. Li, L.M. Sheng, K. An, X.L. Zhao, J. Alloys Compd. **575**, 123 (2013)
3. Y.H. Yu, C.M. Ma, K.C. Yu, C.C. Teng, H.W. Tien, K.Y. Chang, Y.K. Kuo, J. Taiwan Inst. Chem. Eng. **45**, 674 (2014)
4. T.H. Ting, Y.N. Jau, R.P. Yu, Appl. Surf. Sci. **258**, 3184 (2012)
5. M.H. Al-Saleh, W.H. Saadeh, U. Sundararaj, Carbon **60**, 146 (2013)
6. L. Kong, X.W. Yin, X.Y. Yuan, Y.J. Zhang, X.M. Liu, L.F. Cheng, L.T. Zhang, Carbon **73**, 185 (2014)
7. Z. Zou, A.G. Xuan, Z.G. Yan, Y.X. Wu, N. Li, Chem. Eng. Sci. **65**, 160 (2010)
8. G.X. Tong, W.H. Wu, J.G. Guan, H.S. Qian, J.H. Yuan, W. Li, J. Alloys Compd. **509**, 4320 (2011)
9. G.Q. Wang, Y.F. Chang, L.F. Wang, C. Liu, Adv. Powder Technol. **23**, 861 (2012)
10. H. Bayrakar, J. Magn. Magn. Mater. **323**, 1882 (2011)
11. O. Chiscan, I. Dumitru, P. Potolache, V. Tura, A. Stancu, Mater. Lett. **68**, 251 (2012)
12. R.C. Wang, Q. Yu, P. Chen, M.B. Ma, H.L. Chen, Fiber Compos. **3**, 7 (2015)
13. C.J. Li, B. Wang, J.N. Wang, J. Magn. Magn. Mater. **324**, 1305 (2012)
14. J. Xiang, Y.Q. Chu, X.H. Zhang, X.Q. Shen, Appl. Surf. Sci. **263**, 320 (2012)
15. D. Micheli, C. Apollo, R. Pastore, M. Marchetti, Compos. Sci. Technol. **70**, 400 (2010)
16. E.L. Ma, J.J. Li, N.Q. Zhao, E.Z. Liu, C.N. He, C.S. Shi, Mater. Lett. **91**, 209 (2013)
17. X. Zhu, G.Q. Ning, Z.J. Fan, J.S. Gao, C.M. Xu, W.Z. Qian, F. Wei, Carbon **50**, 2764 (2012)
18. T. Wang, H.D. Wang, X. Chi, R. Li, J.B. Wang, Carbon **74**, 312 (2014)
19. J. Xiang, X.H. Zhang, Q. Ye, J.L. Li, X.Q. Shen, Mater. Res. Bull. **60**, 589 (2014)
20. B. Lu, X.L. Dong, H. Huang, X.F. Zhang, X.G. Zhua, J.P. Lei, J.P. Sun, J. Magn. Magn. Mater. **320**, 1106 (2008)